AMERICAN SOCIETY FOR MICROBIOLOGY | Infection and Immunity

Analysis of Endothelial Adherence of *Bartonella henselae* and *Acinetobacter baumannii* Using a Dynamic Human *Ex Vivo* Infection Model

Marko Weidensdorfer,[a] Ju Ik Chae,[a] Celestine Makobe,[a] Julia Stahl,[b] Beate Averhoff,[b] Volker Müller,[b] Christoph Schürmann,[c] Ralf P. Brandes,[c] Gottfried Wilharm,[d] Wibke Ballhorn,[a] Sara Christ,[a] Dirk Linke,[e] Doris Fischer,[f] Stephan Göttig,[a] Volkhard A. J. Kempf[a]

University Hospital, Goethe-University, Institute for Medical Microbiology and Infection Control, Frankfurt am Main, Germany[a]; Department of Molecular Microbiology and Bioenergetics, Institute of Molecular Biosciences, Goethe-University, Frankfurt am Main, Germany[b]; University Hospital, Goethe-University, Institute for Cardiovascular Physiology, Frankfurt am Main, Germany[c]; Robert Koch-Institute, Wernigerode Branch, Wernigerode, Germany[d]; Department of Biosciences, Section for Genetics and Evolutionary Biology, University of Oslo, Oslo, Norway[e]; University Hospital, Goethe-University, Division of Neonatology, Department of Pediatrics, Frankfurt am Main, Germany[f]

Bacterial adherence determines the virulence of many human-pathogenic bacteria. Experimental approaches elucidating this early infection event in greater detail have been performed using mainly methods of cellular microbiology. However, *in vitro* infections of cell monolayers reflect the *in vivo* situation only partially, and animal infection models are not available for many human-pathogenic bacteria. Therefore, *ex vivo* infection of human organs might represent an attractive method to overcome these limitations. We infected whole human umbilical cords *ex vivo* with *Bartonella henselae* or *Acinetobacter baumannii* under dynamic flow conditions mimicking the *in vivo* infection situation of human endothelium. For this purpose, methods for quantifying endothelium-adherent wild-type and trimeric autotransporter adhesin (TAA)-deficient bacteria were set up. Data revealed that (i) *A. baumannii* binds in a TAA-dependent manner to endothelial cells, (ii) this organ infection model led to highly reproducible adherence rates, and furthermore, (iii) this model allowed to dissect the biological function of TAAs in the natural course of human infections. These findings indicate that infection models using *ex vivo* human tissue samples ("organ microbiology") might be a valuable tool in analyzing bacterial pathogenicity with the capacity to replace animal infection models at least partially.

The analysis of adhesion to host cells is crucial for the elucidation of bacterial infection mechanisms. Animal infection models or cellular microbiology-based approaches are well established, and many important findings have thereby been gathered. By way of example, the protein injection machineries and the autotransporter adhesins (TAA) of *Bartonella henselae* and *Acinetobacter baumannii* have been elucidated in that manner (1–3). Although these methods are well established and widely accepted, they still are hampered by several limitations: animal models might reflect the course of human infections only partially (4) or might not even be available for many pathogens (e.g., *B. henselae*). Cellular infection models allow very detailed analyses of the interaction of bacteria with host cells under standardized conditions. However, they are usually done statically using cell monolayers, and this mimics the complexity of *in vivo* infection situation only to some extent. Methods to overcome the species barrier in infection models and to analyze host-pathogen interactions close to the dynamic human situation are urgently needed. *Ex vivo* infection models, using human organ grafts, might represent an attractive alternative or addition to animal or cellular microbiology experiments.

B. henselae causes cat scratch disease and endocarditis, whereas immunosuppressed individuals can suffer from vasculoproliferative disorders such as bacillary angiomatosis. *B. henselae* is believed to be an endotheliotropic pathogen. *Bartonella* adhesin A (BadA) has been identified as the key factor involved in the adherence to endothelial cells (ECs) and to extracellular matrix (ECM) components and in the induction of an angiogenic host cell response (2, 5–7). *A. baumannii* has become an emerging nosocomial pathogen worldwide, mainly in intensive care units. This bacterium is characterized by long-term survival on abiotic surfaces and multidrug resistance to antibiotics (8). After colonization of patients, *A. baumannii* is able to cause bloodstream (including endothelium) infections, urinary tract infections, and ventilator-associated pneumonia (9). Although bloodstream infections with *A. baumannii* are well described (10, 11), nearly nothing is known about the molecular mechanisms underlying the interplay between bacteria and ECs. Different outer membrane-associated proteins are known for *Acinetobacter* adhesion to abiotic surfaces, ECMs, and human host cells for clinical and environmental isolates (12–16). In this context, the *Acinetobacter* trimeric autotransporter adhesin (Ata) is supposed to play a key role in infection processes and adhesion to host cells (3, 17). Unfortunately, not much is known about Ata-dependent interaction of *A. baumannii* with host cells.

The first and often decisive step in bacterial infections is the

Received 11 December 2015 **Accepted** 14 December 2015

Accepted manuscript posted online 28 December 2015

Citation Weidensdorfer M, Chae JI, Makobe C, Stahl J, Averhoff B, Müller V, Schürmann C, Brandes RP, Wilharm G, Ballhorn W, Christ S, Linke D, Fischer D, Göttig S, Kempf VAJ. 2016. Analysis of endothelial adherence of *Bartonella henselae* and *Acinetobacter baumannii* using a dynamic human *ex vivo* infection model. Infect Immun 84:711–722. doi:10.1128/IAI.01502-15.

Editor: A. J. Bäumler

Address correspondence to Volkhard A. J. Kempf, volkhard.kempf@kgu.de.

Supplemental material for this article may be found at http://dx.doi.org/10.1128/IAI.01502-15.

TABLE 1 Bacterial strains used in this study

Strain	Characteristics	Reference(s) or source
B. henselae wild type (BadA$^+$)	Strain Marseille, patient isolate, early passage, expressing BadA	2, 40
B. henselae BadA$^-$	Strain Marseille, transposon mutant, BadA-deficient, Km^r	2
A. baumannii ATCC 19606 wild type	Type strain, isolated from humans, expressing Ata	Gene Bank accession no. ACQB00000000.1
A. baumannii ATCC 19606 Δ*ata*	*ata* markerless deleted mutant (positions 315,815–322,591)	This study
E. coli DH5α	Host strain used for cloning	Biochrom

adherence to the host. TAAs are widely represented in alpha-, beta- and gammaproteobacteria and play an important role in bacterial pathogenicity (18). They are designated autotransporters (or type V secretion systems), as they can self-export across the bacterial outer membrane in the absence of ATP (19). TAAs build a characteristic trimeric, "lollipop"-like surface structure and share a modular organization composed of different domains ("membrane anchor," "stalk," "neck," and "head"), which are conserved modules present in nearly all TAAs (20). Both BadA of *B. henselae* and Ata of A. *baumannii* belong to the group of TAAs and share a similar domain structure architecture. BadA consists of 3,082 amino acids (aa) with a mass of 328 kDa per monomer. The repetitive 22 neck-stalk elements define the enormous length of BadA (~240 nm) (2). Ata is encoded by a 6,786-bp gene. The protein is built up of 2,260 aa and has a mass of 230 kDa per monomer. Characteristic features of Ata are the double-head domain and a long N-terminal signal peptide (see Fig. S1 in the supplemental material).

The aim of this study was to elucidate whether an organ infection model using human umbilical cords might represent a valuable tool to analyze TAA-dependent host adherence of *B. henselae* or *A. baumannii*. The infection procedures were performed under dynamic blood flow mimicking conditions, and methods for the quantification of EC-adherent *B. henselae* and *A. baumannii* were designed (fluorometry and quantitative real-time PCR [qRT-PCR]).

MATERIALS AND METHODS

Bacterial strains. *B. henselae* was grown for 4 days in Schneider's medium supplemented with 10% fetal calf serum (FCS) and 5% sucrose at 37°C in a humidified atmosphere with 5% CO_2 (21). *B. henselae* lacking BadA (BadA$^-$) was grown in the presence of 30 μg/ml kanamycin (Km). Expression analyses for *B. henselae* wild-type and *B. henselae* BadA$^-$ have been performed earlier (2, 22). Stock suspensions were prepared by freezing the bacteria in lysogeny broth (LB) containing 20% glycerol at −80°C. The number of viable bacteria per aliquot was determined by counting the CFU in serial dilutions from the frozen stocks, which were cultivated on Columbia blood agar (CBA) plates for 14 days. *A. baumannii* was grown in 2× yeast extract-tryptone (YT) medium and incubated at 37°C and 180 rpm overnight. The optical density at 600 nm (OD_{600}) was adjusted to 0.05 in 2× YT medium, and bacteria were regrown to an OD_{600} of 0.2 (1.0×10^8 CFU/ml) for infection experiments. Strains used in this study are summarized in Table 1.

Construction of *A. baumannii* Δ*ata*. The construction of an *ata* deletion mutant of *A. baumannii* ATCC 19606 was performed according to a method by Stahl and Averhoff (23), using the plasmids and primers listed in Tables 2 and 3, respectively. We constructed a vector containing a 1.5-kbp fragment both up- and downstream from the *ata* gene. For this, up- and downstream fragments (here termed up-fragment and down-fragment, respectively) were amplified from genomic DNA using primers *ata*_up_PstI_fwd/*ata*_up_BamHI_rev and *ata*_down_BamHI-fwd/*ata*_down_NotI_rev. Both fragments were digested (up-fragment, PstI/BamHI; down-fragment, BamHI/NotI) and ligated into pBIISK (digested with PstI/NotI), resulting in pBIISK_*ata*_up/down. This plasmid was transformed into *A. baumannii* ATCC 19606 by electroporation. The resulting clones were selected on LB agar supplemented with 50 μg/ml kanamycin. Transformed bacteria were grown overnight in LB medium containing 10% sucrose to select cells that lost the plasmid after homologous recombination. Integration of homologous regions was proven by colony PCR using *ata*_ctrl_fwd and *ata*_ctrl_rev. The next day, single colonies were picked and transferred to LB agar and LB agar supplemented with 50 μg/ml kanamycin to finally identify the colonies that had lost the plasmid (no growth on LB agar supplemented with kanamycin). Successful deletion of *ata* was verified by sequencing using *ata*_seq_fwd and *ata*_seq_rev (data not shown).

Infection of endothelial cells and confocal laser scanning microscopy. Human umbilical vein endothelial cells (HUVECs) were cultured in EC growth medium (PromoCell, Mannheim, Germany) as described previously (24). For static adherence assays, 1.0×10^5 HUVECs were seeded onto collagen G (Biochrom, Hamburg, Germany)-coated coverslips in 24-well plates, grown overnight without antibiotics, and infected with a multiplicity of infection (MOI) of 100 for *B. henselae* or 200 for *A. baumannii* by centrifugation (300 × *g*, 5 min). Cells were incubated for 60 min in a humidified atmosphere at 37°C and 5% CO_2. After a gentle washing with prewarmed cell culture medium, the infection was stopped by adding 3.75% paraformaldehyde (PFA). For quantification of adherent bacteria by fluorometry and qRT-PCR, 5×10^5 cells were seeded (in six-well plates) and infection was done as described above.

TABLE 2 Plasmids used in this study

Plasmid	Characteristics	Resistance	Source
TOPO_TA_2.1	Standard cloning vector for amplicons with TA-overhangs, *lacZ*α for blue/white screening	Km^r Amp^r	Thermo Fisher Scientific
TOPO_TA_2.1_*glyA*	TOPO_TA.2.1 including *glyA* fragment	Km^r Amp^r	This study
TOPO_TA_2.1_*rpoB*	TOPO_TA.2.1 including *rpoB* fragment	Km^r Amp^r	This study
TOPO_TA_2.1_*hmbs*	TOPO_TA.2.1 including *hmbs* fragment	Km^r Amp^r	This study
pBluescript II SK(+) (pBIISK)	Cloning vector for *A. baumannii* ATCC 19606, *sacB* (levansucrase) for segregation	Km^r	Stratagene
pBIISK_*ata*_up/down	pBIISK including the 1.5-kbp *ata*_up and 1.5-kbp *ata*_down fragments	Km^r	This study

TABLE 3 Primers used in this study

Primer	5′→3′ sequence	Source or reference
*glyA*_fwd	GAC AGG AAA ATG TGC CGA AT	This study
*glyA*_rev	GCA GGT GAA CCA AGA CGA AT	This study
*rpob*_fwd	GAG TCT AAT GGC GGT GGT TC	41
*rpob*_rev	ATT GCT TCA TCT GCT GGT TG	41
*hmbs*_fwd	TTC CTT CCC TGA AGG GAT TCA CTC AG	Galaxy Diagnostics, Durham, NC, USA
*hmbs*_rev	TTA AGC CCA GCA GCC TAT CTG ACA CCC	Galaxy Diagnostics, Durham, NC, USA
*ata*_up_PstI_fwd	GAC ACT GCA GCA TTT AGA AAG TAT TCA CGT TGG TTC	This study
*ata*_up_BamHI_rev	GAT CGG ATC CCT TTA TTC ATA AAA CTT CTC AGA C	This study
*ata*_down_BamHI_fwd	GAG AGG ATC CGA AAC TGG TTA GGA GGG CAA TGC TC	This study
*ata*_down_NotI_rev	GAC AGC GGC CGC GAT TTC TCC ATG AAT GAA TTA AG	This study
*ata*_ctrl_fwd	GTC CAA CCA AGC AAA GGA TAG GGC CTT TGA G	This study
*ata*_ctrl_rev	CTA ACT GAT CTA AAA ATT CAC CAA TTT TTC GG	This study
*ata*_seq_fwd	GTC GTT GAG TTC GGT ATT TGT CTG AGA AG	This study
*ata*_seq_rev	TAA TCT CTT TAA TCT GTC AGC AAG GAG AGC	This study

For dynamic adherence assays, HUVECs (100 μl of a 1.0×10^6 cell suspension) were seeded overnight in growth medium without antibiotics on collagen G-coated multichannel slides (Ibidi, Martinsried, Germany). Bacteria were resuspended in 12 ml EC growth medium (MOI of 100 for *B. henselae* or 200 for *A. baumannii*), and HUVECs were infected with a constant flow rate of 0.2 ml (~0.26 dyne/cm^2 [1 dyne is 10^{-5} N], according to the manufacturer's indications)/min for 60 min. After a gentle washing with prewarmed cell culture medium for 5 min, the infection was stopped by adding 3.75% PFA and microscopic slides were prepared. When adherent bacteria were quantified, cells were dissolved by adding trypsin-EDTA (Gibco BRL-Invitrogen, Karlsruhe, Germany), flushed with EC medium, and collected in 15-ml Falcon tubes.

Bacterial adherence was quantified using confocal laser scanning microscopy (CLSM) as described previously (24). Cells were permeabilized by incubation with 0.1% Triton X-100 (Sigma, Steinheim, Germany) in phosphate-buffered saline (PBS) for 15 min. The actin cytoskeleton was stained with tetramethylrhodamine isothiocyanate (TRITC)-labeled phalloidin (Sigma, Steinheim, Germany) for 1 h, and EC and bacterial DNA was stained with 4′,6-diamidin-2′-phenylindole dihydrochloride (DAPI) for 10 min. Finally, slides were mounted with Fluoprep medium (bioMérieux, Marcy l'Etoile, France). Cellular fluorescence was evaluated using a Leica DM IRE 2 confocal laser scanning microscope. Images were digitally processed with Photoshop 7.0 (Adobe Systems, Mountain View, CA).

Dynamic adhesion assay using human umbilical cords. All experiments were done in accordance with ethical permission (4/12; University Hospital Frankfurt am Main). Human umbilical cords were collected in the midwifery of the Klinikum Sachsenhausen (Frankfurt am Main, Germany). Autolytic or otherwise affected samples were omitted from further experiments. For infection, fresh human umbilical cord veins were cut into two pieces of ~5 cm in length each for comparison of wild-type and mutant bacteria. Veins were connected with buttoned cannulas, fixed with cable binders, and washed with prewarmed EC culture medium (0.2 ml/min, 15 min). Bacterial suspensions were prepared as described above and adjusted to 1.0×10^8 CFU/ml in prewarmed EC culture medium. The infection was started by switching a three-way valve and injecting the bacteria into the umbilical cord vein by a pump. Samples were continuously infected for 60 min in a recirculating system (Fig. 1). After this, nonadherent bacteria were flushed by washing the veins with EC cell culture medium. For determination of adherent bacteria, ECs were removed by injecting prewarmed 0.05% trypsin–EDTA into the vein and incubating the sample for 10 min. Dissolved cells were washed out of the veins and collected in 15-ml Falcon tubes for further processing.

Microcomputed tomography, shear stress calculation, and Doppler analysis. For *ex vivo* microcomputed tomography (CT) imaging, the umbilical cord vein was perfused with PBS and a three-way valve connected to polyethylene tubing was introduced. The vein was perfused with the radiopaque contrast solution MicroFil (Flow Tech, Carver, MA, USA) with a pressure of 10 to 15 mm Hg until the silicon polymer cured. The umbilical cords were subsequently scanned in a micro-CT (Skyscan 1176; Bruker micro-CT, Kontich, Belgium) with the following settings: 50 kV; 0.5-mm aluminum filter; 500-μA source current; exposure time, 210 ms; 18-μm isotopic resolution; 3 projection images per 0.5° rotation step; rotation range, 180°. Volumetric data were reconstructed with the NRecon/InstaRecon CBR Server—Premium software (Skyscan, Kontich, Belgium/InstaRecon, Champaign, IL, USA). Image analysis, segmentation of micro-CT data, and quantification of vein lumen area were performed with the Imalytics Preclinical Software (Gremse-IT, Aachen, Germany). Discrimination of contrast agent and soft tissue was achieved by applying a threshold defined as the mean of contrast agent and soft tissue intensity. The lumen area of the vein was measured with the virtual elastic sphere tool (25) (Fig. 2A). Shear stress (τ) was calculated according to the following formula: $\tau = (4 \times \mu \times \nu)/(\pi \times r^3)$, where μ is the viscosity (1.011 mPa × s), ν is the flow rate (3.3×10^{-9} m^3/s), and r is the diameter (26).

To confirm laminar flow conditions in the umbilical cord vein during infection procedures, ultrasound Doppler analysis was performed. The flow pattern was recorded using a linear ultrasound head (5 to 12 MHz; here 9 MHz) connected with a Phillips Envisor ultrasound device (Hamburg, Germany) while the vein was flushed with 10% barium sulfate (resuspended in PBS). A monodirectional laminar flow with a flow velocity directly corresponding to the infusion pump velocity for 10% barium sulfate (0.2 ml/min, resuspended in PBS) was detectable (Fig. 2B).

Quantification of endothelial cell-adherent bacteria by fluorometry. For fluorometric quantification of bacterial adherence to ECs, bacteria were stained with the life-staining dye carboxyfluorescein succinimidyl ester (CFSE; Santa Cruz biotechnology, Heidelberg, Germany) prior to infection. Bacteria were grown as described above, centrifuged for 10 min at 10,000 × *g*, washed with PBS (Gibco), and resuspended in 10 μM CFSE (dissolved in PBS) for 15 min at 37°C. CFSE-stained bacteria were washed with PBS. Potential bactericidal effects were excluded by comparing the amounts of CFU prior to and after the labeling procedures, which revealed no significant reduction of bacterial viability (quantified by determination of CFU; data not shown).

To correlate the total number of CFSE-labeled adherent bacteria to the total number of ECs, cells were labeled with anti-CD31-Alexa 647-conjugated antibodies. PFA-fixed ECs were incubated with 0.2% bovine serum albumin (BSA; dissolved in PBS) to block unspecific antibody binding. ECs were washed with PBS and incubated with 10 μg of anti-CD31-Alexa Fluor 647 (dissolved in PBS) for 60 min at room temperature and protected from light. Nonbound antibodies were removed by washing the cells with PBS.

For quantification of the EC-adherent bacteria, total cell samples from

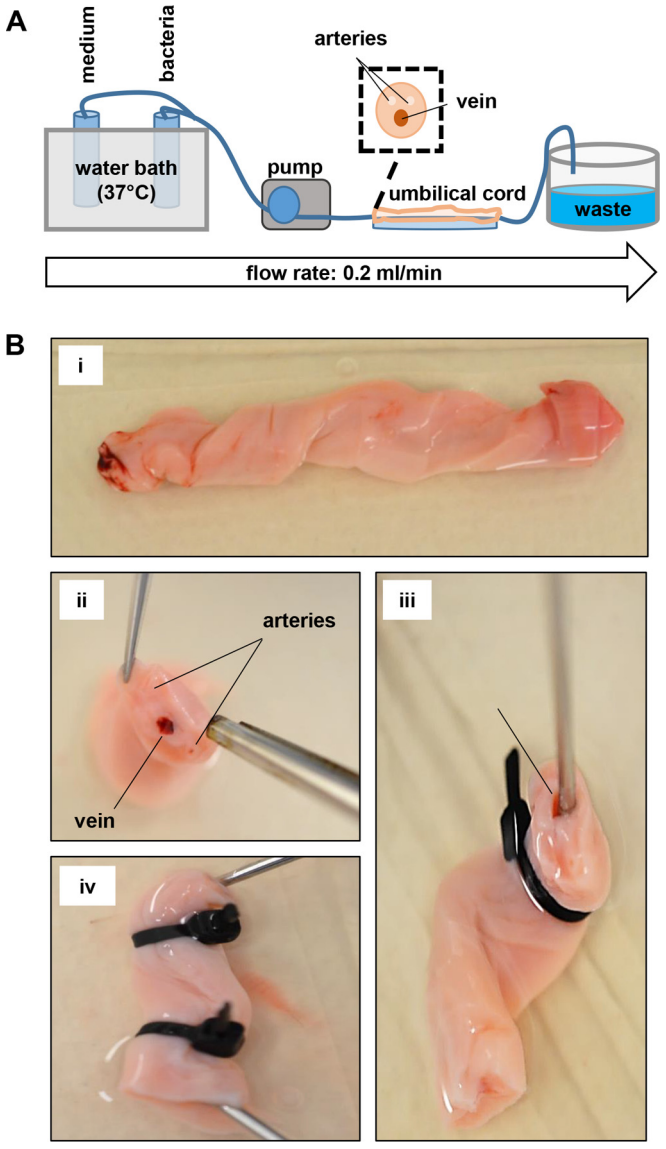

FIG 1 Experimental setup of the *ex vivo* umbilical cord infection assays. (A) Schematic draft of the experimental setup. A pump is connected with a fresh human umbilical cord vein. Blood clots and debris are flushed by pumping prewarmed medium through the vein for 15 min. Bacteria were pumped in prewarmed medium for 60 min with a constant defined flow (0.2 ml/min). After this, nonadherent bacteria were removed by flushing the vein for an additional 15 min with prewarmed medium. (B) Photography of processing of human umbilical cords for *ex vivo* infections: (i) fresh umbilical cord of ~10 cm in length; (ii) situs of a cross-section of the umbilical cord (note the umbilical vein); (iii and iv) connection of buttoned cannulas (arrow) (iii), which were fixed (iv) by using cable binders.

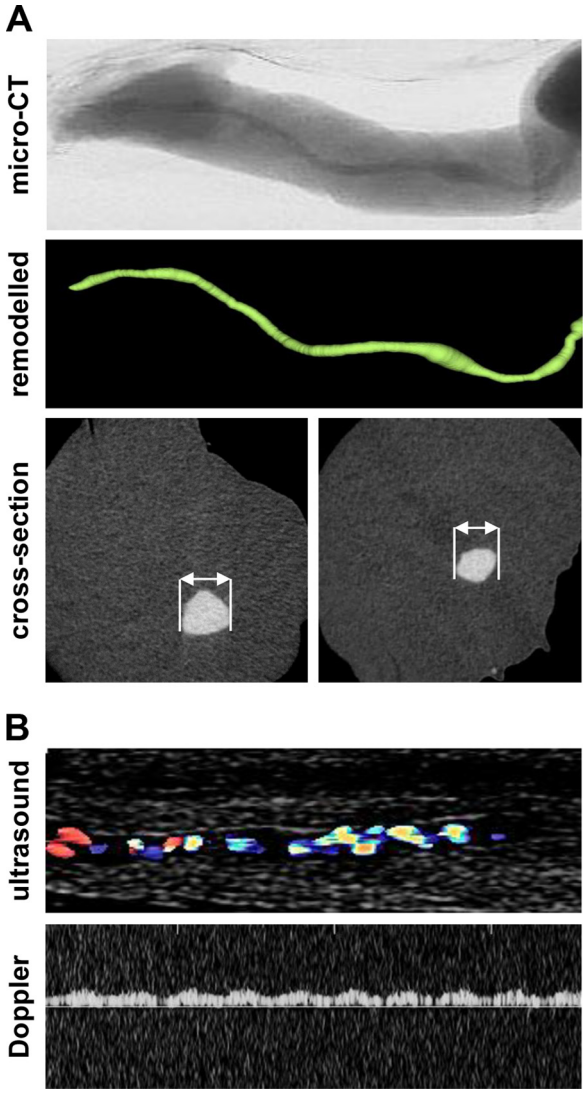

FIG 2 Microcomputed tomography and Doppler ultrasound analysis of umbilical cord veins. (A) Umbilical cord veins were perfused with MicroFil contrast solution, recorded by microcomputed tomography, and digitally processed; total length analyzed, 1.8 cm; diameter, 1.3 (left) or 0.9 (right) mm. (B) For ultrasound analysis, umbilical cord veins were washed and infected with barium sulfate (10%, resuspended in PBS).

infection experiments (including CFSE bacteria and CD31-Alexa Fluor 647 HUVECs) were dispersed in 200 μl PBS, and the total volume was added to a black 96-well plate (Greiner BioOne GmbH, Frickenhausen, Germany). Additionally, standards were prepared: for CFSE-labeled bacteria, 1.0×10^5 to 1.0×10^7 CFU/well; for CD31-Alexa Fluor 647-labeled ECs, 1.0×10^4 to 1.0×10^6 cells/well. Calibration was performed by standard methods: bacterial CFU were calculated from cultivating serial dilutions on agar plates, and ECs were quantified using a Thoma cell counting chamber. Quantification of the relative fluorescence units (RFU) was performed using a multiple plate reader (Infinite 200 PRO; Tecan, Männedorf, Switzerland). The adjusted emission and excitation wavelengths for CFSE were 482 nm and 517 nm, and for Alexa Fluor 674, 647 nm and 678 nm, respectively. A standard curve was calculated by the internal standard in each experiment, and absolute bacterial and EC amounts were determined.

Quantification of endothelial cell-adherent bacteria by quantitative real-time PCR. To quantify the number of adherent bacteria and HUVECs by using numbers of gene copy equivalents, qRT-PCRs were established. Samples (not PFA fixed) were prepared as described above, centrifuged (10,000 × *g*, 10 min), and dissolved in 30 μl distilled water. DNA was isolated by incubating the cells for 15 min at 95°C. After this, samples were centrifuged again at 10,000 × *g* for 10 min to remove cellular debris. DNA concentration was determined via 260 nm/280 nm photometry. The determination of bacterial and EC numbers was performed by determining gene copy numbers. The isolated genomic DNA of the samples was used to amplify species-specific genes. For quantifying adherent *B. henselae* isolates, a *glyA* (serine hydroxymethyltransferase, 120-bp)

gene fragment was used, and for quantifying adherent *A. baumannii*, an *rpoB* (RNA polymerase beta-subunit, 110 bp) gene fragment was used. To determine the amount of ECs, the *hmbs* (hydroxymethylbilane synthase, 209 bp) gene was amplified. Primers are given in Table 3. DNA samples were added in a qRT-PCR mixture (5 μl qRT-PCR-SYBR green master mix [Qiagen, Hilden, Germany] together with 0.125 μl of forward and reverse primers [each 100 pmol] and 2.75 μl distilled water). For each qRT-PCR, an internal standard with known gene copy numbers was amplified. These PCR standards were produced by amplifying the respective gene fragments of *glyA*, *rpoB*, and *hmbs* and ligation into a TOPO_TA_2.1 vector according to the manufacturer's instructions (Thermo Fisher Scientific, Waltham, MA, USA). Total copy numbers of the resulting plasmids were calculated using the molecular mass of the single plasmids, the plasmid concentration, and the Avogadro constant ($N_A = 6 \times 10^{23}$ mol^{-1}) according to the following formula: plasmid copy number = $N_A \times m/M$, where m is the plasmid mass after isolation in grams and M is the molecular mass of plasmids in grams per mole. For calculation of adherent bacteria per EC, the following formula was used: binding ratio (bacteria/EC) = bacterial gene equivalent (*rpoB*, *glyA*)/0.5 EC gene equivalent (*hmbs*).

Statistical analysis and bioinformatics. All experiments were performed at least three times. Differences between mean values of experimental and control groups were analyzed by Student's *t* test (Graph Pad Prism 4.03; Graph Pad Software, San Diego, CA, USA). A *P* value of <0.05 was considered to be statistically significant.

RESULTS

The aim of this study was to establish a new *ex vivo* organ infection model for analyzing bacterial adherence and to investigate whether Ata-dependent mechanisms of *A. baumannii* interactions with ECs are principally existing. For this approach, human umbilical cord veins were used, and adhesion of TAA-expressing and -deficient *B. henselae* and *A. baumannii* was analyzed. Quantification of adherent bacteria was done by fluorometry and qRT-PCR.

Quantification of bacterial adherence to ECs using fluorometry and quantitative qRT-PCR. Adhesion of *B. henselae* to ECs is usually determined by counting cell-adherent bacteria, e.g., via fluorescence microscopy (2). It is obvious that such procedures—although they might be of use when working with slow-growing bacteria—are time-consuming and suffer from interobserver variability. Therefore, methods independent from microscopy or cultivation techniques might be useful for determining bacterial adherence. We established two independent technologies to overcome these limitations by using fluorometry and qRT-PCR analysis to quantify the adherent bacteria.

For fluorometric analysis, bacteria were stained with CFSE, and ECs were labeled with an anti-CD31-Alexa Fluor 647 antibody (see Materials and Methods), resulting in a bright green fluorescence of the stained bacteria and a bright orange fluorescence of the labeled ECs in fluorescence microscopy (data not shown). As emission and excitation spectra do not overlap, fluorescence was clearly distinguishable by fluorometry. The numbers of labeled bacteria (*B. henselae* and *A. baumannii*) and ECs showed a strict linear correlation with relative fluorescence units (RFU); the correlation coefficients were 0.978 (*B. henselae*), 0.989 (*A. baumannii*), and 0.993 (ECs) (Fig. 3).

For the determination of bacterial adherence by the quantification of genome equivalents, a qRT-PCR method was developed. Therefore, specific primers for bacteria were designed (for *B. henselae*, targeting *glyA*; for *A. baumannii*, targeting *rpoB*) resulting in specific amplicons of 120 bp and 110 bp, respectively. For EC-specific amplicons, an *hmbs* PCR was used (209 bp) (Table 3). All primers were tested and found not to result in unspecific amplicons within the described setting (data not shown). The generation of internal standards was done by ligation of the respective amplicons into TOPO_TA vectors and transformation into *Escherichia coli* DH5α, and the correct insertion of the fragments was verified by PCR and restriction fragment length polymorphism (RFLP) (data not shown). Plasmids were propagated in *E. coli* DH5α, and the respective plasmid copy number was determined as described above (see Materials and Methods). Using these internal standards (from 10 to 10^6 copies), a linear correlation between threshold cycle (C_T) values and log copy number was observed (Fig. 3). Correlation coefficients were 0.946 (*B. henselae*), 0.993 (*A. baumannii*), and 0.997 (ECs).

TAA-dependent adherence of *B. henselae* and *A. baumannii* to ECs under static infection conditions. To analyze the TAA-dependent attachment of *B. henselae* and *A. baumannii* to ECs, HUVECs were infected as described above for 60 min. Adherence was determined via fluorescence microscopy, and as expected, BadA-expressing *B. henselae* adhered to ECs whereas *B. henselae* BadA$^-$ showed a clearly reduced cell adherence (Fig. 4A). Fluorescence microscopy findings correlated with those obtained by fluorometry or qRT-PCR (Fig. 4B). For wild-type *B. henselae*, ~25.3 ± 5.5 adherent bacteria (by fluorometry) or ~35.4 ± 1.8 bacteria per HUVEC (by qRT-PCR) were calculated. Binding rates were significantly reduced when HUVECs were infected with *B. henselae* BadA$^-$ (~6.0 ± 1.5 bacteria [fluorometry] or ~17.2 ± 1.6 bacteria per HUVEC [qRT-PCR]). To address the role of Ata in binding to ECs, an *ata* deletion mutant was constructed as described in Materials and Methods. It turned out that the presence or absence of Ata correlated with bacterial binding to ECs. As observed by fluorescence microscopy, total numbers of adherent bacteria were lower than numbers of *B. henselae* (Fig. 4C). These data were confirmed by fluorometry (wild type, ~4.6 ± 1.1 bacteria per HUVEC) and qRT PCR (~8.7 ± 0.4 bacteria per HUVEC) (Fig. 4D). EC adherence of Ata-deficient *A. baumannii* was significantly reduced (~1.8 ± 0.4 bacteria [fluorometry] and ~0.6 ± 0.1 bacteria [qRT PCR] per HUVEC). Taken together, loss of BadA or Ata expression resulted in an ~3-fold (*B. henselae*) or ~6-fold (*A. baumannii*) reduction in adherence to ECs.

TAA-dependent adherence of *B. henselae* and *A. baumannii* to ECs under dynamic infection conditions. Next, we used the dynamic infection models to analyze the role of TAA-mediated EC binding under shear stress conditions (0.26 dyne/cm^2). Here, only very few adherent bacteria (both *B. henselae* and *A. baumannii*) were detectable by fluorescence microscopy, indicating strongly reduced bacterial adherence under shear stress conditions (Fig. 5A and C). These observations were confirmed by fluorometry and qRT-PCRs: ~1.4 ± 0.2 *B. henselae* wild-type isolates (fluorometry) and ~13.6 ± 1.2 bacteria (qRT-PCR) adhered per HUVEC (Fig. 5B and D). For *B. henselae* BadA$^-$, only ~0.5 ± 0.1 bacteria (fluorometry) and ~1.2 ± 0.5 bacteria (qRT-PCR) adhered to HUVECs. Similar results were obtained when analyzing dynamic EC binding of *A. baumannii* (Fig. 5D): for the wild type, ~1.6 ± 0.2 bacteria (fluorometry) and ~0.7 ± 0.1 bacteria (qRT-PCR) per HUVEC; for Ata-deficient bacteria, ~0.2 ± 0.1 bacteria (fluorometry) and ~0.1 ± 0.02 bacteria (qRT-PCR) per HUVEC. In summary, under dynamic infection conditions, TAA-deficient bacteria showed a more reduced EC adherence than under static infection conditions (*B. henselae*, ~9-fold reduction; *A. baumannii*, ~8-fold reduction).

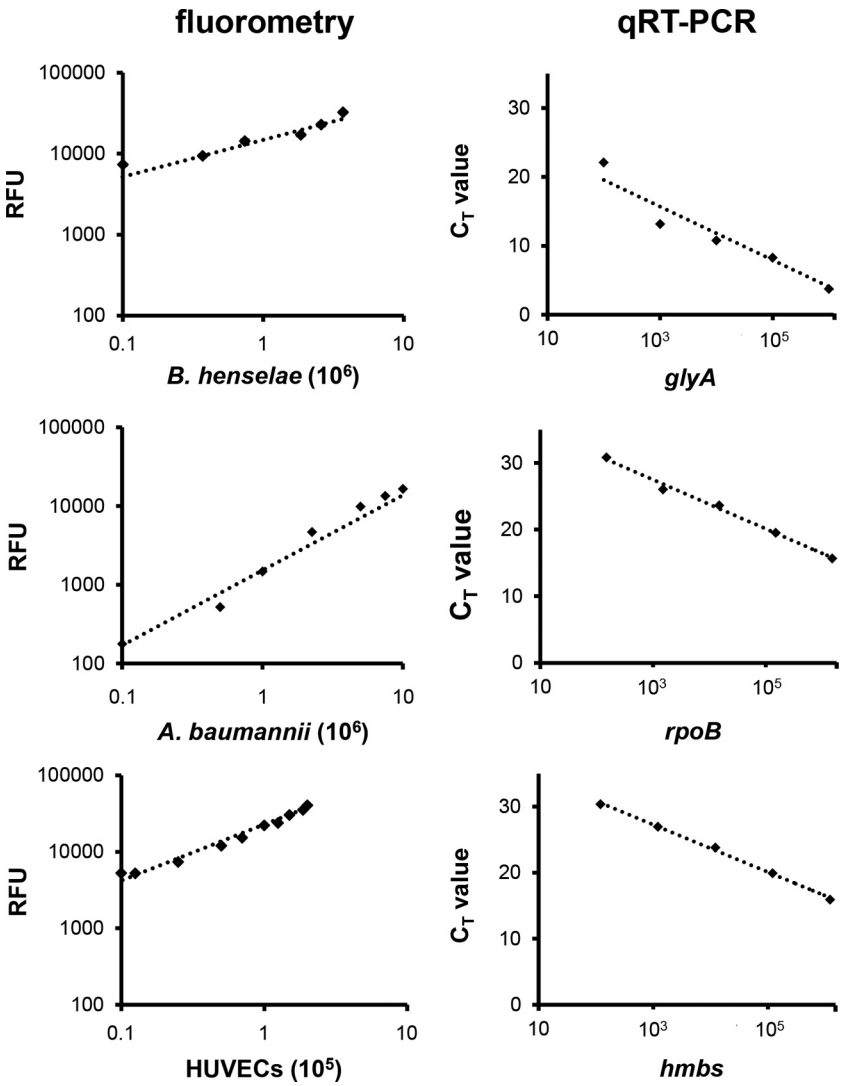

FIG 3 Quantification of bacteria and ECs using fluorometry or qRT-PCR. (Left) Correlation between bacterial CFSE- or EC-anti-CD31 fluorescence intensity quantified by fluorometry. *y* axis, relative fluorescence units (RFU). (Right) Correlation between C_T values (*y* axis) of the respective amplified (log copy number, *x* axis) bacterial (*B. henselae glyA*; *A. baumannii rpoB*) or endothelial (*hmbs*) genes.

TAA-dependent adherence of *B. henselae* and *A. baumannii* to human umbilical cord endothelial cells *ex vivo*. Finally, we transferred the infection procedures in an *ex vivo* organ infection model using human umbilical cords. Fresh human whole-organ grafts were prepared and dynamically infected with *B. henselae* and *A. baumannii* strains as described above. As the micro-CT revealed an umbilical cord vein with a diameter of 4.0 ± 0.6 mm ($n = 20$) (Fig. 2A), the mean shear stress was calculated at 0.5 ± 0.2 dyne/cm^2. Moreover, flow pattern analysis via ultrasound and Doppler revealed a unidirectional and laminar flow (Fig. 2B). Fluorescence microscopy analysis of vessel samples (taken after 60 min of infection) (Fig. 6A and C) demonstrated TAA-dependent binding of *B. henselae* and *A. baumannii* to human endothelium to a certain degree. However, counting of EC-adherent bacteria was not feasible because of limitations in fluorescence microscopy due to the thickness of the microscopic samples. In contrast, fluorometry and qRT-PCR technology allowed to calculate the number of adherent bacteria in this *ex vivo* organ infection model. Here, total binding rates for *B. henselae* wild-type strain were ~2.4 ± 0.9 bacteria (fluorometry) and ~14.3 ± 3.6 bacteria (qRT-PCR) per EC. *B. henselae* BadA$^-$ showed a ~3-fold-lower adhesion: ~0.50 ± 0.08 bacteria (fluorometry) and ~6.3 ± 1.8 bacteria (qRT-PCR) attached per human EC (Fig. 6B). For wild-type *A. baumannii*, ~2.3 ± 0.4 bacteria (fluorometry) and ~7.3 ± 0.3 bacteria (qRT-PCR) adhered per EC, whereas, in contrast, *A. baumannii* Ata$^-$ showed a ~4-fold-lower adhesion (~0.20 ± 0.08 bacteria [fluorometry] and ~2.4 ± 0.6 bacteria [qRT-PCR] per EC) (Fig. 6D). Notably, total binding rates of *B. henselae* were similar to those obtained in the dynamic *in vitro* approach and those of *A. baumannii* were ~4-fold higher.

DISCUSSION

Adhesion of pathogenic bacteria to host cells is an early step for establishing an infection. Elucidating the details of how the bacteria attach to host cells is of great interest in infection biology research because it allows to understand this crucial pathogenicity

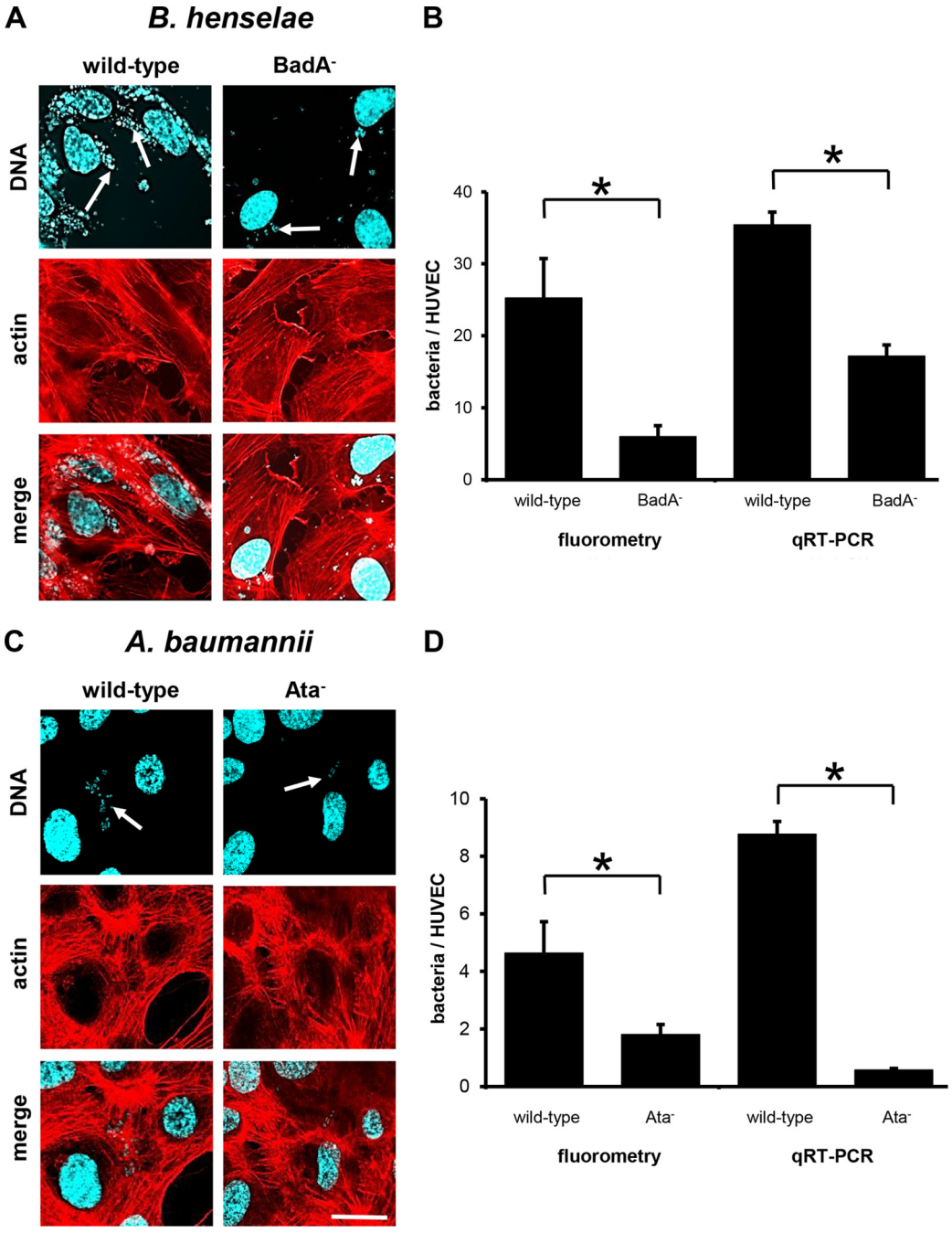

FIG 4 TAA-dependent adhesion of *B. henselae* and *A. baumannii* to HUVECs (static infection). HUVECs (1.0×10^5) were seeded on coverslips and infected with the respective bacteria (for *B. henselae* at an MOI of 100; for *A. baumannii* at an MOI of 200) for 60 min. For fluorescence microscopy (A, C), actin cytoskeleton of ECs was stained with TRITC-phalloidin (red), bacteria and nuclei were stained with DAPI (blue), and images were digitally overlaid (merge). Scale bar, 20 μm. (B, D) Adherence to ECs was determined in parallel by using fluorometry and qRT-PCRs. *, $P < 0.05$.

mechanism. Moreover, such analyses might help to prevent infections by, e.g., identifying promising vaccination targets or via inhibiting adhesion to host cells by "antiligands." These two strategies are getting more and more important as many pathogenic and multidrug-resistant Gram-negative bacteria (e.g., *A. baumannii*) have emerged in the last decade (27, 28).

The aim of our study was to develop an infection model that mimics infection conditions closer to those encountered in nature as previously used in *in vitro* approaches. For this purpose, we set up a dynamic human organ infection model using human umbilical cord veins. This model was proven to render reliable results in bacterial adherence for the two emerging pathogens *B. henselae* and *A. baumannii*.

Determination of bacterial adherence by fluorometry and qRT-PCR. For the quantification of adherent bacteria, we set up two independent approaches based on fluorometry and qRT-

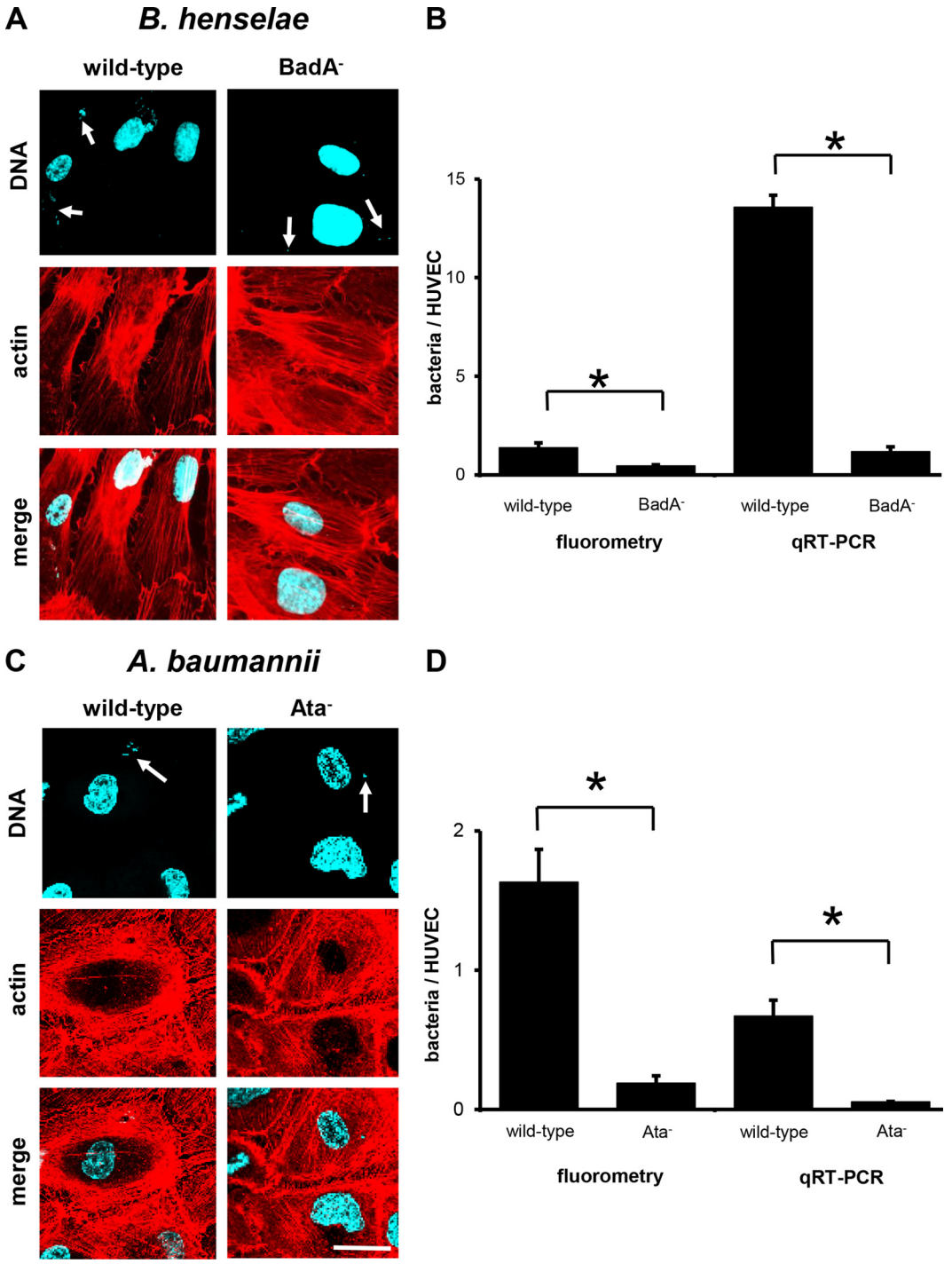

FIG 5 TAA-dependent adhesion of *B. henselae* and *A. baumannii* to HUVECs (dynamic conditions). HUVECs (1.0×10^4) were seeded on multichannel slides and infected with 1.0×10^8 bacteria per ml under constant flow conditions (flow rate, 0.2 ml per min) for 15 min (*B. henselae*) or 60 min (*A. baumannii*). (A, C) For fluorescence microscopy, actin cytoskeleton of ECs was stained with TRITC-phalloidin (red), bacteria and nuclei were stained with DAPI (blue), and images were digitally overlaid (merge). Scale bar, 20 μm. (B, D) Adherence to ECs was determined in parallel by using fluorometry and qRT-PCR. *, $P < 0.05$.

PCR. Principally, our results revealed that fluorometry is an easy and valuable tool in analyzing bacterial adherence rates. We found that this method is highly reproducible, showing a linear correlation between the number of CFSE-stained bacteria or antibody-labeled ECs and the respective relative fluorescence units (Fig. 3). Using internal standards for fluorometry, the number of bacteria and cells was determinable, allowing to calculate the absolute number of adherent bacteria per endothelial cell. Further advantages are that no specific antibodies are needed for bacterial labeling and that adhesion of slow-growing bacteria like *B. henselae* to

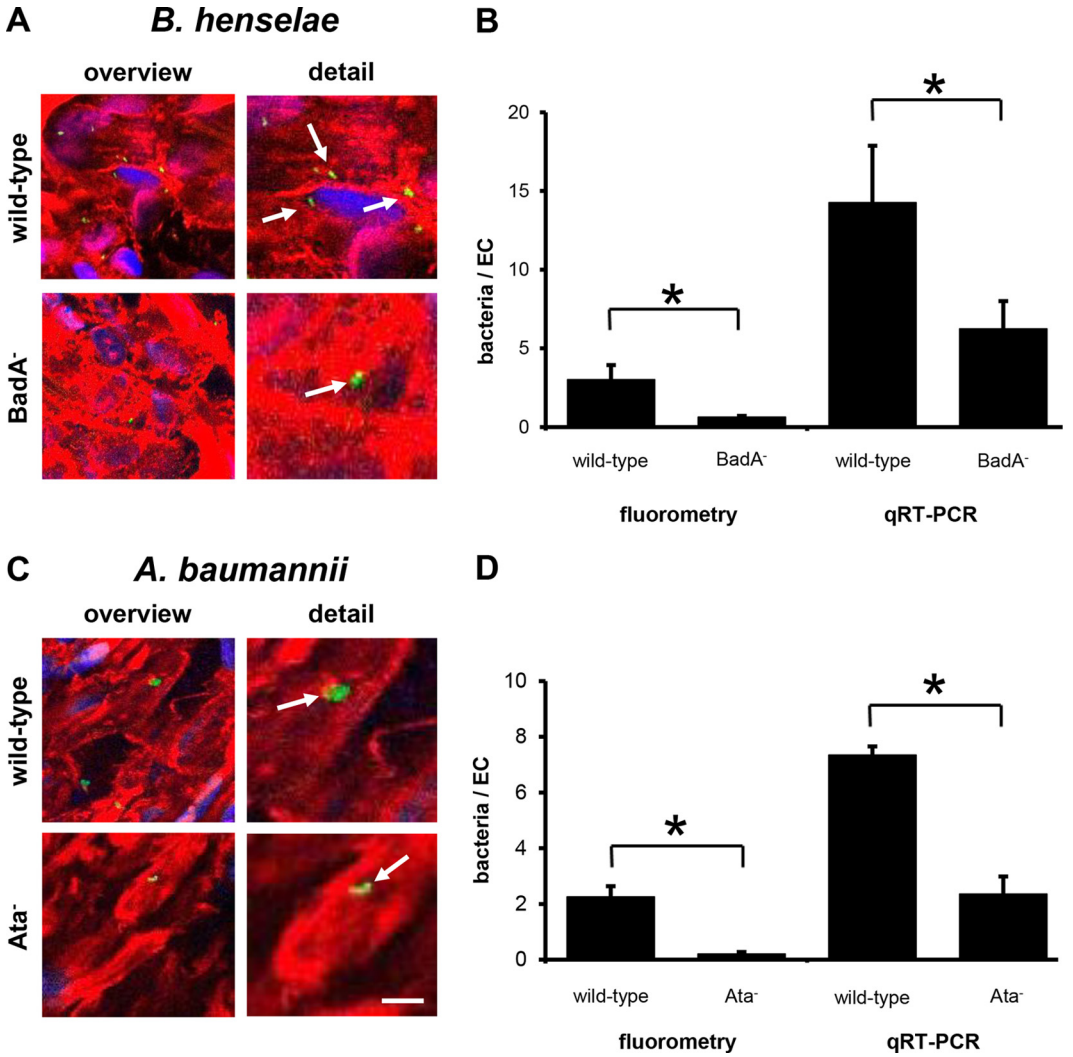

FIG 6 TAA-dependent adhesion of *B. henselae* and *A. baumannii* to human umbilical cord endothelial cells *ex vivo*. Human umbilical cord veins were infected for 60 min as described in Materials and Methods. (A, C) For fluorescence microscopy, actin cytoskeleton of ECs was stained with TRITC-phalloidin (red), bacteria were stained with CFSE (green) prior to infection, and nuclei were stained with DAPI (blue). Scale bar, 10 μm. (B, D) Adherent bacteria were quantified by using fluorometry (B) and qRT-PCRs (D). *, $P < 0.05$.

ECs can be analyzed within hours instead of weeks by omitting long-lasting bacterial subcultivation. CD31 (also known as platelet/endothelial cell adhesion molecule-1 [PECAM-1]) was used as a marker for ECs (29). It can be suggested that our fluorometry approach might be expanded to other cell types, since many specific cell antibodies are available (e.g., to lymphatic vessels specifically expressing the lymphatic vessel marker 1 [LYVE-1]) (30). Furthermore, bacterial adherence to host cells could be quantified using a qRT-PCR approach by determining the number of bacterial and host cell genome equivalents. This method was highly reproducible and also showed a linear correlation between the number of bacteria or ECs and the C_T values of the specific amplified fragments. Using internal plasmid standards for qRT-PCR, the absolute number of adherent bacteria per EC can be determined.

In our study, the detection limits of fluorometry (upcoming background signals of PBS and unstained cells) are 50,000 bacteria and 5,000 ECs (Fig. 3). Therefore, this method is helpful in experiments in which such bacterial or host cell numbers can be expected. In contrast, qRT-PCR-based determination of adherence is more sensitive by nature (the limit of detection was one bacterium or one host cell). This method is more useful for experiments in which low numbers of bound bacteria are expected. Notably, the two methods revealed comparable results. In the case of *B. henselae*, e.g., under static infection conditions, ~25 bacteria per EC were detected via fluorometry whereas ~35 bacteria were calculated from qRT-PCR. These data are congruent to those from our earlier observations (2, 6). In the case of *A. baumannii*, ~5 bacteria were found to be adherent to ECs by fluorometry and ~9 bacteria via qRT-PCR. We conclude that both methods might expand the spectrum of methods in adherence research in future, as they might be adapted to many adherence assays with some minor modifications.

Notably, fluorescence microscopy of tissue samples (e.g., hu-

man umbilical cord tissue) is difficult by nature: on the one hand, the sample is relatively thick (>1 mm), and on the other hand, the so-called "Wharton's jelly" (*substantia gelatina funiculi umbilicalis*), which is the major structure component of the umbilical cord, prevents reliable fluorescence microscopy. Here, fluorometry and qRT-PCR-based bacterial quantification are clearly superior to microscopic techniques when analyzing bacterial adherence. The use of "multiphoton microscopy" might overcome such limitations, as thicker tissue samples (>1 mm) can be analyzed (31); however, such microscopes are highly expensive and of limited access.

TAA-dependent adherence of *B. henselae* and *A. baumannii*. Since the role of BadA in mediating bacterial adherence to ECs has been analyzed in detail (2, 5, 6, 32, 33), *B. henselae* was used in our study as a control to calibrate the experiments with *A. baumannii*. Previous works described mainly Ata-dependent adhesion abilities of *A. baumannii* to ECMs under static infection conditions (3). In contrast, not much is known about the role of Ata in mediating the binding of *A. baumannii* to host cells, especially to ECs, or in a dynamic infection model. It is highly likely that at least in systemic infections (e.g., bloodstream infections) *A. baumannii* bacteria will interact with human endothelium (10, 11); however, this process has not been analyzed in detail. Therefore, our data show for the first time that Ata mediates in fact the binding of *A. baumannii* to human ECs. Our study revealed a ~5-fold-higher binding of *A. baumannii* wild type to ECs than of isogenic Ata deletion mutants under static infection conditions. When ECs were infected under shear stress conditions, the binding rate decreased significantly. In static infection assays, ~7 wild-type bacteria and ~1 Ata-deficient bacterium attached to the ECs, whereas under shear stress the binding rates decreased to ~1 wild-type bacterium and ~0.2 Ata-deficient *A. baumannii* isolate. Interestingly, the binding rates to ECs of *A. baumannii* are much lower than those of *B. henselae* (see above). It can be assumed that the binding to ECs is much more pronounced in *B. henselae*, as this pathogen is an endotheliotropic bacterium (33). In contrast, ECs might not represent the typical target cells in *A. baumannii* infections, since this pathogen targets mainly respiratory and skin epithelia (34). Consequently, the exact molecular basis for endothelial or epithelial tropism of *A. baumannii* and the binding affinities still remain to be elucidated.

Infection of human tissue grafts: a step toward "organ microbiology." Cell culture-based static infection models are widely accepted in cellular microbiology and pathogenicity research. Recently, dynamic cellular and live murine infection models have been applied for analyzing the interaction of bacteria with ECs *in vitro* or using intravital microscopy, e.g., for *B. henselae*, *Bartonella quintana*, *Yersinia enterocolitica*, *Neisseria meningitidis*, *Borrelia burgdorferi*, and *Staphylococcus aureus* (6, 35–38). Although these methods are of high importance in the field of pathogenicity research, they suffer from some shortcomings by nature: (i) dynamic *in vitro* adherence assays are restricted to one particular cell line in an artificial experimental environment (lacking the complexity of natural human tissues; e.g., cell-cell-adhesions, extracellular matrices, mixed cell types, elasticity of human blood vessels) and (ii) cell growth conditions (addition of growth factors, fetal calf serum, etc.) or passaging of the cells might lead to unexpected cellular differentiation patterns influencing the specific characteristics of human cell lines (39); moreover, (iii) intravital microscopy is laborious and also limited to animal, mostly murine infection models. In the case of *B. henselae*, no appropriate murine infection model exists. Thus, alternative experimental settings are needed (33). Moreover, murine infection models (e.g., pneumonia models [3, 17]) might be limited in transferability to humans (4).

To overcome these restrictions, we developed a new infection model for analyzing bacterial adherence using human umbilical cords and shear stress conditions to mimic the human bloodstream conditions. Umbilical cord veins are suitable tools for this for many reasons: high disposability, the constant flow and shear stress allowed by the laminar structure of the veins, ethical acceptance, and the avoidance of animal infection experiments. We demonstrate that our infection model mimics the physiological shear stress of ~0.5 dyne/cm^2 and unidirectional laminar fluid flow in venous vessels. Similar conditions are found in the human blood circulation system (26), and thus our model is close to nature. Using this model, we demonstrated as a "proof of principle" that TAA-dependent adherence to ECs can be analyzed under dynamic flow infection conditions. Our experiments revealed for wild-type *B. henselae* total binding rates of ~9.0 bacteria and for *B. henselae* BadA$^-$ up to ~3.0 bacteria per EC (Fig. 6A and B). For *A. baumannii*, total binding rates were lower than for *B. henselae*; however, the Ata-deficient mutant showed ~4-fold-lower adhesion rates than wild-type bacteria (Fig. 6C and D). Compared to dynamic *in vitro* infection settings, endothelial *ex vivo* bacterial adhesion was generally ~2-fold higher. This might be caused by more-physiological additional binding sites in the human umbilical cord veins.

The work described here demonstrates that dynamic *ex vivo* infection models using human umbilical cords might represent a new, valuable tool in infection biology. Together with the calculation of adherent bacteria via fluorometry and qRT-PCR, this method has already allowed to analyze the role of the TAAs BadA and Ata in the infection process of human endothelial cells. Further studies with this newly developed infection model could allow detailed investigations of, e.g., host cell responses during dynamic infection procedures under more-physiological conditions. These findings might have the potential to expand the technologies present in "cellular microbiology" to a seminal new field in infection biology ("organ microbiology").

ACKNOWLEDGMENTS

We thank Horst Buxmann and Rolf L. Schlößer (Department of Neonatology, University Hospital Frankfurt am Main), the midwife team from the Hospital Frankfurt Sachsenhausen for ensuring the support with fresh human umbilical cords, and Evelyn Skiebe for excellent technical assistance.

FUNDING INFORMATION

This work was supported by grants from the Deutsche Forschungsgemeinschaft (DFG-FOR 2251 to V. Kempf, S. Göttig, B. Averhoff, G. Wilharm, and V. Müller and DFG-SFB 815 to V. Kempf and R. Brandes).

REFERENCES

1. **Schülein R, Seubert A, Gille C, Lanz C, Hansmann Y, Piemont Y, Dehio C.** 2001. Invasion and persistent intracellular colonization of erythrocytes: a unique parasitic strategy of the emerging pathogen *Bartonella*. J Exp Med **193:**1077–1086. http://dx.doi.org/10.1084/jem.193.9.1077.
2. **Riess T, Andersson SG, Lupas A, Schaller M, Schäfer A, Kyme P, Martin J, Wälzlein J-H, Ehehalt U, Lindroos H, Schirle M, Nordheim A, Autenrieth IB, Kempf VA.** 2004. *Bartonella* adhesin A mediates a proan-

giogenic host cell response. J Exp Med **200:**1267–1278. http://dx.doi.org/10.1084/jem.20040500.
3. **Bentancor LV, Camacho-Peiro A, Bozkurt-Guzel C, Pier GB, Maira-Litran T.** 2012. Identification of Ata, a multifunctional trimeric autotransporter of *Acinetobacter baumannii*. J Bacteriol **194:**3950–3960. http://dx.doi.org/10.1128/JB.06769-11.
4. **Seok J, Warren HS, Cuenca AG, Mindrinos MN, Baker HV, Xu W, Richards DR, McDonald-Smith GP, Gao H, Hennessy L, Finnerty CC, Lopez CM, Honari S, Moore EE, Minei JP, Cuschieri J, Bankey PE, Johnson JL, Sperry J, Nathens AB, Billiar TR, West MA, Jeschke MG, Klein MB, Gamelli RL, Gibran NS, Brownstein BH, Miller-Graziano C, Calvano SE, Mason PH, Cobb JP, Rahme LG, Lowry SF, Maier RV, Moldawer LL, Herndon DN, Davis RW, Xiao W, Tompkins RG.** 2013. Genomic responses in mouse models poorly mimic human inflammatory diseases. Proc Natl Acad Sci U S A **110:**3507–3512. http://dx.doi.org/10.1073/pnas.1222878110.
5. **Kempf VA, Lebiedziejewski M, Alitalo K, Walzlein JH, Ehehalt U, Fiebig J, Huber S, Schütt B, Sander CA, Müller S, Grassl G, Yazdi AS, Brehm B, Autenrieth IB.** 2005. Activation of hypoxia-inducible factor-1 in bacillary angiomatosis: evidence for a role of hypoxia-inducible factor-1 in bacterial infections. Circulation **111:**1054–1062. http://dx.doi.org/10.1161/01.CIR.0000155608.07691.B7.
6. **Müller NF, Kaiser PO, Linke D, Schwarz H, Riess T, Schäfer A, Eble JA, Kempf VA.** 2011. Trimeric autotransporter adhesin-dependent adherence of *Bartonella henselae*, *Bartonella quintana*, and *Yersinia enterocolitica* to matrix components and endothelial cells under static and dynamic flow conditions. Infect Immun **79:**2544–2553. http://dx.doi.org/10.1128/IAI.01309-10.
7. **O'Rourke F, Mändle T, Urbich C, Dimmeler S, Michaelis UR, Brandes RP, Flotenmeyer M, Döring C, Hansmann ML, Lauber K, Ballhorn W, Kempf VA.** 2015. Reprogramming of myeloid angiogenic cells by *Bartonella henselae* leads to microenvironmental regulation of pathological angiogenesis. Cell Microbiol **17:**1447–1463. http://dx.doi.org/10.1111/cmi.12447.
8. **Göttig S, Gruber TM, Higgins PG, Wachsmuth M, Seifert H, Kempf VA.** 2014. Detection of pan drug-resistant *Acinetobacter baumannii* in Germany. J Antimicrob Chemother **69:**2578–2579. http://dx.doi.org/10.1093/jac/dku170.
9. **Dijkshoorn L, Nemec A, Seifert H.** 2007. An increasing threat in hospitals: multidrug-resistant *Acinetobacter baumannii*. Nat Rev Microbiol **5:**939–951. http://dx.doi.org/10.1038/nrmicro1789.
10. **Seifert H, Strate A, Pulverer G.** 1995. Nosocomial bacteremia due to *Acinetobacter baumannii*: clinical features, epidemiology, and predictors of mortality. Medicine **74:**340–349. http://dx.doi.org/10.1097/00005792-199511000-00004.
11. **Sebeny PJ, Riddle MS, Petersen K.** 2008. *Acinetobacter baumannii* skin and soft-tissue infection associated with war trauma. Clin Infect Dis **47:**444–449. http://dx.doi.org/10.1086/590568.
12. **Brossard KA, Campagnari AA.** 2012. The *Acinetobacter baumannii* biofilm-associated protein plays a role in adherence to human epithelial cells. Infect Immun **80:**228–233. http://dx.doi.org/10.1128/IAI.05913-11.
13. **Gaddy JA, Tomaras AP, Actis LA.** 2009. The *Acinetobacter baumannii* 19606 OmpA protein plays a role in biofilm formation on abiotic surfaces and in the interaction of this pathogen with eukaryotic cells. Infect Immun **77:**3150–3160. http://dx.doi.org/10.1128/IAI.00096-09.
14. **Smani Y, McConnell MJ, Pachón J.** 2012. Role of fibronectin in the adhesion of *Acinetobacter baumannii* to host cells. PLoS One **7:**e33073. http://dx.doi.org/10.1371/journal.pone.0033073.
15. **Eijkelkamp BA, Stroeher UH, Hassan KA, Paulsen IT, Brown MH.** 2014. Comparative analysis of surface-exposed virulence factors of *Acinetobacter baumannii*. BMC Genomics **15:**1020. http://dx.doi.org/10.1186/1471-2164-15-1020.
16. **Ishikawa M, Nakatani H, Hori K.** 2012. AtaA, a new member of the trimeric autotransporter adhesins from *Acinetobacter* sp. Tol 5 mediating high adhesiveness to various abiotic surfaces. PLoS One **7:**e48830. http://dx.doi.org/10.1371/journal.pone.0048830.
17. **Bentancor LV, Routray A, Bozkurt-Guzel C, Camacho-Peiro A, Pier GB, Maira-Litran T.** 2012. Evaluation of the trimeric autotransporter Ata as a vaccine candidate against *Acinetobacter baumannii* infections. Infect Immun **80:**3381–3388. http://dx.doi.org/10.1128/IAI.06096-11.
18. **Linke D, Riess T, Autenrieth IB, Lupas A, Kempf VA.** 2006. Trimeric autotransporter adhesins: variable structure, common function. Trends Microbiol **14:**264–270. http://dx.doi.org/10.1016/j.tim.2006.04.005.
19. **Leo JC, Grin I, Linke D.** 2012. Type V secretion: mechanism(s) of autotransport through the bacterial outer membrane. Philos Trans R Soc Lond B Biol Sci **367:**1088–1101. http://dx.doi.org/10.1098/rstb.2011.0208.
20. **Lyskowski A, Leo JC, Goldman A.** 2011. Structure and biology of trimeric autotransporter adhesins. Adv Exp Med Biol **715:**143–158. http://dx.doi.org/10.1007/978-94-007-0940-9_9.
21. **Riess T, Dietrich F, Schmidt KV, Kaiser PO, Schwarz H, Schäfer A, Kempf VA.** 2008. Analysis of a novel insect cell culture medium-based growth medium for *Bartonella* species. Appl Environ Microbiol **74:**5224–5227. http://dx.doi.org/10.1128/AEM.00621-08.
22. **Kaiser PO, Linke D, Schwarz H, Leo JC, Kempf VA.** 2012. Analysis of the BadA stalk from *Bartonella henselae* reveals domain-specific and domain-overlapping functions in the host cell infection process. Cell Microbiol **14:**198–209. http://dx.doi.org/10.1111/j.1462-5822.2011.01711.x.
23. **Stahl J, Bergmann H, Göttig S, Ebersberger I, Averhoff B.** 2015. *Acinetobacter baumannii* virulence is mediated by the concerted action of three phospholipases D. PLoS One **10:**e0138360. http://dx.doi.org/10.1371/journal.pone.0138360.
24. **Kempf VA, Schaller M, Behrendt S, Volkmann B, Aepfelbacher M, Cakman I, Autenrieth IB.** 2000. Interaction of *Bartonella henselae* with endothelial cells results in rapid bacterial rRNA synthesis and replication. Cell Microbiol **2:**431–441. http://dx.doi.org/10.1046/j.1462-5822.2000.00072.x.
25. **Gremse F, Grouls C, Palmowski M, Lammers T, de Vries A, Grull H, Das M, Muhlenbruch G, Akhtar S, Schober A, Kiessling F.** 2011. Virtual elastic sphere processing enables reproducible quantification of vessel stenosis at CT and MR angiography. Radiology **260:**709–717. http://dx.doi.org/10.1148/radiol.11110069.
26. **Malek AM, Alper SL, Izumo S.** 1999. Hemodynamic shear stress and its role in atherosclerosis. JAMA **282:**2035–2042. http://dx.doi.org/10.1001/jama.282.21.2035.
27. **Gruber TM, Göttig S, Mark L, Christ S, Kempf VA, Wichelhaus TA, Hamprecht A.** 2015. Pathogenicity of pan-drug-resistant *Serratia marcescens* harbouring blaNDM-1. J Antimicrob Chemother **70:**1026–1030. http://dx.doi.org/10.1093/jac/dku482.
28. **Göttig S, Gruber TM, Stecher B, Wichelhaus TA, Kempf VA.** 2015. *In vivo* horizontal gene transfer of the carbapenemase OXA-48 during a nosocomial outbreak. Clin Infect Dis **60:**1808–1815. http://dx.doi.org/10.1093/cid/civ191.
29. **Miettinen M, Lindenmayer AE, Chaubal A.** 1994. Endothelial cell markers CD31, CD34, and BNH9 antibody to H- and Y-antigens: evaluation of their specificity and sensitivity in the diagnosis of vascular tumors and comparison with von Willebrand factor. Mod Pathol **7:**82–90.
30. **Jackson DG.** 2003. The lymphatics revisited: new perspectives from the hyaluronan receptor LYVE-1. Trends Cardiovasc Med **13:**1–7. http://dx.doi.org/10.1016/S1050-1738(02)00189-5.
31. **Werkmeister E, Kerdjoudj H, Marchal L, Stoltz JF, Dumas D.** 2007. Multiphoton microscopy for blood vessel imaging: new non-invasive tools (Spectral, SHG, FLIM). Clin Hemorheol Microcirc **37:**77–88.
32. **Lu YY, Franz B, Truttmann MC, Riess T, Gay-Fraret J, Faustmann M, Kempf VA, Dehio C.** 2013. *Bartonella henselae* trimeric autotransporter adhesin BadA expression interferes with effector translocation by the VirB/D4 type IV secretion system. Cell Microbiol **15:**759–778. http://dx.doi.org/10.1111/cmi.12070.
33. **Kaiser PO, Riess T, O'Rourke F, Linke D, Kempf VA.** 2011. *Bartonella* spp.: throwing light on uncommon human infections. Int J Med Microbiol **301:**7–15. http://dx.doi.org/10.1016/j.ijmm.2010.06.004.
34. **Visca P, Seifert H, Towner KJ.** 2011. *Acinetobacter* infection: an emerging threat to human health. IUBMB Life **63:**1048–1054. http://dx.doi.org/10.1002/iub.534.
35. **Soyer M, Dumenil G.** 2012. A laminar-flow chamber assay for measuring bacterial adhesion under shear stress. Methods Mol Biol **799:**185–195. http://dx.doi.org/10.1007/978-1-61779-346-2_12.
36. **Claes J, Liesenborghs L, Lox M, Verhamme P, Vanassche T, Peetermans M.** 2015. *In vitro* and *in vivo* model to study bacterial adhesion to the vessel wall under flow conditions. J Vis Exp **100:**e52862. http://dx.doi.org/10.3791/52862.
37. **Laschke MW, Kerdudou S, Herrmann M, Menger MD.** 2005. Intravital fluorescence microscopy: a novel tool for the study of the interaction of *Staphylococcus aureus* with the microvascular endothelium *in vivo*. J Infect Dis **191:**435–443. http://dx.doi.org/10.1086/427193.
38. **Moriarty TJ, Norman MU, Colarusso P, Bankhead T, Kubes P, Chaconas G.** 2008. Real-time high resolution 3D imaging of the Lyme disease spirochete

adhering to and escaping from the vasculature of a living host. PLoS Pathog **4:**e1000090. http://dx.doi.org/10.1371/journal.ppat.1000090.
39. **Hartung T.** 2013. Food for thought look back in anger—what clinical studies tell us about preclinical work. ALTEX **30:**275–291. http://dx.doi.org/10.14573/altex.2013.3.275.
40. **Drancourt M, Birtles R, Chaumentin G, Vandenesch F, Etienne J, Raoult D.** 1996. New serotype of *Bartonella henselae* in endocarditis and cat-scratch disease. Lancet **347:**441–443. http://dx.doi.org/10.1016/S0140-6736(96)90012-4.
41. **Hornsey M, Ellington MJ, Doumith M, Thomas CP, Gordon NC, Wareham DW, Quinn J, Lolans K, Livermore DM, Woodford N.** 2010. AdeABC-mediated efflux and tigecycline MICs for epidemic clones of *Acinetobacter baumannii*. J Antimicrob Chemother **65:**1589–1593. http://dx.doi.org/10.1093/jac/dkq218.